Prion disease tempo determined by host-dependent substrate reduction

Charles E. Mays, … , David Westaway, Jiri G. Safar

Research Article **Neuroscience**

The symptoms of prion infection can take years or decades to manifest following the initial exposure. Molecular markers of prion disease include accumulation of the misfolded prion protein (PrP^{Sc}), which is derived from its cellular precursor (PrP^{C}), as well as downregulation of the PrP-like Shadoo (Sho) glycoprotein. Given the overlapping cellular environments for PrP^{C} and Sho, we inferred that PrP^{C} levels might also be altered as part of a host response during prion infection. Using rodent models, we found that, in addition to changes in PrP^{C} glycosylation and proteolytic processing, net reductions in PrP^{C} occur in a wide range of prion diseases, including sheep scrapie, human Creutzfeldt-Jakob disease, and cervid chronic wasting disease. The reduction in PrP^{C} results in decreased prion replication, as measured by the protein misfolding cyclic amplification technique for generating PrP^{Sc} in vitro. While PrP^{C} downregulation is not discernible in animals with unusually short incubation periods and high PrP^{C} expression, slowly evolving prion infections exhibit downregulation of the PrP^{C} substrate required for new PrP^{Sc} synthesis and as a receptor for pathogenic signaling. Our data reveal PrP^{C} downregulation as a previously unappreciated element of disease pathogenesis that defines the extensive, presymptomatic period for many prion strains.

Find the latest version:

Prion disease tempo determined by host-dependent substrate reduction

Charles E. Mays,[1] Chae Kim,[2,3] Tracy Haldiman,[2]
Jacques van der Merwe,[1] Agnes Lau,[1] Jing Yang,[1] Jennifer Grams,[1]
Michele A. Di Bari,[4] Romolo Nonno,[4] Glenn C. Telling,[5] Qingzhong Kong,[2,3]
Jan Langeveld,[6] Debbie McKenzie,[1,7] David Westaway,[1,7] and Jiri G. Safar[2,3,8]

[1]Centre for Prions and Protein Folding Diseases, University of Alberta, Edmonton, Alberta, Canada.
[2]National Prion Disease Surveillance Center and [3]Department of Pathology, School of Medicine, Case Western Reserve University,
Cleveland, Ohio, USA. [4]Department of Veterinary Public Health and Food Safety, Istituto Superiore di Sanità, Rome, Italy.
[5]Prion Research Center and Department of Microbiology, Immunology and Pathology, College of Veterinary Medicine and Biomedical Sciences,
Colorado State University, Fort Collins, Colorado, USA. [6]Central Veterinary Institute of Wageningen UR, Lelystad, The Netherlands.
[7]Department of Biological Sciences, Division of Neurology, and Department of Biochemistry, University of Alberta, Edmonton, Alberta, Canada.
[8]Department of Neurology, School of Medicine, Case Western Reserve University, Cleveland, Ohio, USA.

The symptoms of prion infection can take years or decades to manifest following the initial exposure. Molecular markers of prion disease include accumulation of the misfolded prion protein (PrP^{Sc}), which is derived from its cellular precursor (PrP^C), as well as downregulation of the PrP-like Shadoo (Sho) glycoprotein. Given the overlapping cellular environments for PrP^C and Sho, we inferred that PrP^C levels might also be altered as part of a host response during prion infection. Using rodent models, we found that, in addition to changes in PrP^C glycosylation and proteolytic processing, net reductions in PrP^C occur in a wide range of prion diseases, including sheep scrapie, human Creutzfeldt-Jakob disease, and cervid chronic wasting disease. The reduction in PrP^C results in decreased prion replication, as measured by the protein misfolding cyclic amplification technique for generating PrP^{Sc} in vitro. While PrP^C downregulation is not discernible in animals with unusually short incubation periods and high PrP^C expression, slowly evolving prion infections exhibit downregulation of the PrP^C substrate required for new PrP^{Sc} synthesis and as a receptor for pathogenic signaling. Our data reveal PrP^C downregulation as a previously unappreciated element of disease pathogenesis that defines the extensive, presymptomatic period for many prion strains.

Introduction

Prions are transmissible agents responsible for incurable neurodegenerative diseases in humans and animals. Infection with prions is unique in that they may manifest after a lag phase that can exceed 5 decades from the time of exposure (1). The generation of infectivity from recombinant prion protein (PrP) (2) supports the "protein-only" hypothesis, whereby prion replication corresponds to a conformational transition from the host-encoded, cellular prion protein (PrP^C) substrate into a misfolded infectivity-associated form called PrP^{Sc}. Initiation of prion disease has an obligatory dependence upon the introduction of a PrP^{Sc} "seed," and susceptibility to disease is blocked by PrP gene null alleles (3). Prion disease pathogenesis is associated with a progressive accumulation of PrP^{Sc} levels, with the qualification that PrP^{Sc} may encompass subforms that are biophysically and perhaps toxicologically distinct (4, 5).

Besides PrP^C, the Shadoo (Sho) glycoprotein is also expressed in the central nervous system. Sho has a similarity to the N-terminal region of PrP (6, 7) and interacts with several proteins that also interact with PrP^C (8). While the function of Sho remains to be determined, a notable discovery was that levels of the Sho protein are reduced (downregulated) in prion disease (7, 9). Since this effect is apparent in the preclinical phase of disease (10, 11), we speculated that this phenomenon might be of broader importance for pathogenesis. In particular, the status of

PrP^C protein levels during prion infection has been investigated little, because of the unaltered steady-state levels of the corresponding mRNA (12, 13) and a co-occurrence of PrP^{Sc} that may be present in molar excess. Here, to investigate PrP^C, while avoiding the confounding presence of PrP^{Sc}, velocity gradient centrifugation was used to separate monomeric PrP^C from oligomeric and high molecular assemblies containing PrP^{Sc} (14). We then applied the conformation-dependent immunoassay (CDI), which measures a "hidden" epitope of PrP^{Sc} subsequent to its exposure by use of a chemical denaturant. By means of this 2-step procedure, we were able to analyze levels of different PrP species, including PrP^C, protease-resistant PrP^{Sc} (rPrP^{Sc}), and protease-sensitive PrP^{Sc} (sPrP^{Sc}) (5). Our studies demonstrated both quantitative and qualitative alterations in PrP^C, with a number of implications for our understanding of prion disease pathogenesis.

Results

PrP^C downregulation at end stage in scrapie, Creutzfeldt-Jakob disease, and chronic wasting disease models. The procedure to couple velocity gradient centrifugation with CDI (as explained in the Introduction) has been validated previously for samples derived from hamsters (5) and humans (15). To extend this approach to the analysis of mouse PrP, we recalibrated conditions for the use of the monoclonal antibody 12B2 (mouse PrP epitope at residues 88–92) (ref. 16 and Figure 1, A and B). We then applied the recalibrated technique to the analysis of mouse brain homogenates; these homogenates were derived from WT mouse brains harvested at clinical end stage after infection with the Rocky Mountain Laboratory (RML) iso-
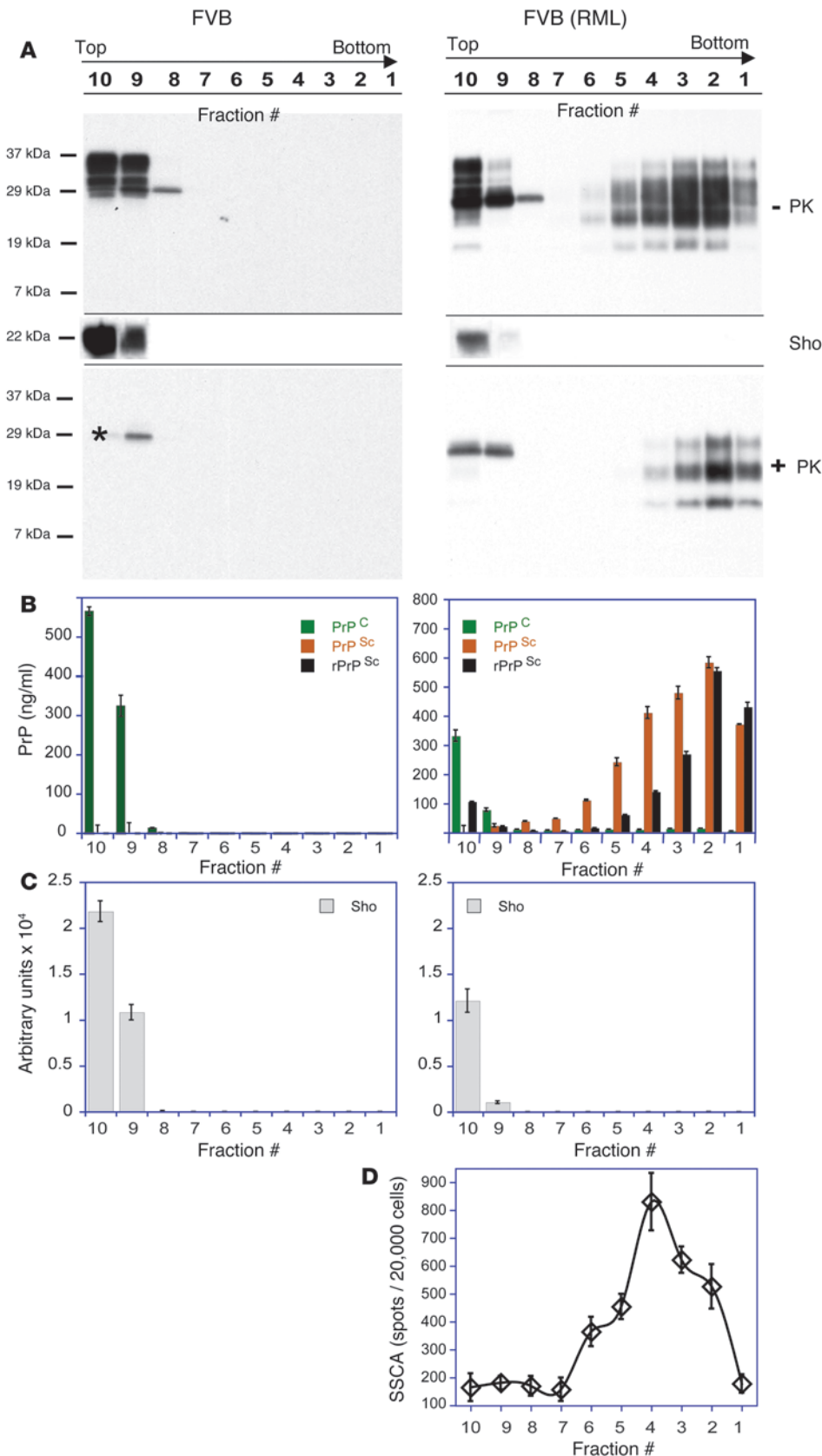
Figure 1
Separation of PrP isoforms and prion infectivity by sedimentation velocity in sucrose gradient. (**A**) The gradient fractionation profile of PrPs present in uninfected brain homogenates of WT FVB mice compared to that of those infected with the RML scrapie isolate strain after separation by ultracentrifugation in sucrose gradient. Fractions collected from the bottom of the tubes were treated with PK or left untreated and analyzed by (**A**) Western blot using anti-PrP mAb 12B2 and (**B**) CDI. Protein marker mass is shown in kDa for Western blots, and the asterisk indicates cross-reactivity between secondary antibody and IgG light chain present in the brain homogenates. The concentration of PrP^C (green), total PrP^{Sc} (brown), and rPrP^{Sc} (black) in fractions from triplicate samples was determined with CDI with Eu-labeled mAb 12B2 before or after PK treatment (14). (**C**) Densitometry analysis of the Western blot signal for Sho was estimated with ImageJ. (**D**) SSCA performed in L929 cells to estimate infectivity in gradient-fractionated RML prions. Data for uninfected animals appears on the left and that for RML-infected animals appears on the right. Data represent average ± SEM

late of mouse-adapted scrapie prions. Our analyses demonstrated that 93% of the upper gradient fractions, fractions 9 and 10, are composed of PrP^C, while rPrP^Sc and sPrP^Sc make up the remaining 7% (Figure 1B). Since PrP^C is the predominant PrP isoform, we attempted to use the protein within these gradient fractions as a substrate in an in vitro assay to make PrP^Sc; this assay procedure is called protein misfolding cyclic amplification (PMCA) and is conceptually similar to PCR amplification of nucleic acids. However, proteins within the upper fractions of the velocity gradients were incompatible with our PMCA conditions and showed no detectable amplification, even though the levels of PrP^C and concentrations of PrP^Sc after seeding with infected brain homogenate were comparable to the PMCA control experiment with nonfractionated material (Supplemental Figure 1; see complete unedited blots in the supplemental material; supplemental material available online with this article; doi:10.1172/JCI72241DS1). Nonetheless, the low infectivity of these fractions, as determined by the standard scrapie cell assay (SSCA; a cell monolayer assay to determine the infectious titer for prions), supports the notion that the major component of these upper fractions is indeed PrP^C (Figure 1D). In comparing RML prion-infected and noninfected animals, we discovered that total PrP^C levels were decreased by 41% ($P < 0.001$) (Figure 1B). Interestingly, the PrP-like protein Sho was found in the same gradient fractions as PrP^C, where it was also reduced in the RML-infected animals by approximately 48% of control values ($P < 0.001$) (Figure 1, A and C).

To determine whether PrP^C downregulation is a broad-spectrum characteristic of prion infection, we applied similar analysis to end-stage brain material derived from WT mice infected with different strains of prions. Prion strains are microbiological isolates with distinct pathogenic properties that "breed true"; in molecular terms, they are thought to correspond to differently folded isoforms of PrP^Sc (17). For this purpose, we examined WT mice challenged with the 22L or 139A strains of scrapie prions, Syrian hamsters inoculated with the Sc237 scrapie prion strain, Tg cervid PrP (TgCe) mice (18) inoculated with chronic wasting disease (CWD) prions, Tg human PrP (TgHu) mice (19) challenged with a strain of human sporadic Creutzfeldt Jakob Disease (sCJD) prions, and bank voles inoculated with bank vole–adapted CWD prions. Our further analyses also included mice with a different genetic makeup. The most common allele of the mouse PrP gene (*Prnp*) is the *Prnp^a* allele encoding PrP^C-A. Here, we performed RML bioassays using mice that produce different levels of PrP^C-A, which correspond to Tg mice expressing 0.53 times endogenous PrP^C-A levels of WT mice (Tg*Prnp^a*-AL mice) and Tg*Prnp^a* mice (a widely used Tg, commonly referred to as *tga20*) overexpressing PrP^C-A by approximately 6-fold (20). Excluding Tg*Prnp^a* mice and bank voles, marked decreases ($P < 0.001$) were noted in the net PrP^C (primarily present in fractions 9 and 10 in infected brains; Supplemental Figures 1–6), and these decreases ranged from 31% ± 3.9% to 68% ± 8.4% (± SEM) (Figure 2). As described for analyses with the RML prion isolate, Sho protein colocalized in fractions 9 and 10 with PrP^C in 22L- and 139A-infected brain material from WT mice at levels 42%–48% of the control values (22L strain, $P < 0.001$; 139A strain, $P < 0.01$) (Supplemental Figure 1C).

PrP^C quality is altered by prion infection. For the 3 scrapie strains analyzed in WT mice (Figure 1A and Supplemental Figure 1A), we were surprised to discover that residual PrP^C present in infected animals exhibited an altered glycosylation profile. Generally, diglycosylated forms were underrepresented, and there were increased levels of

Table 1
Relationship between expression rate of mouse PrP^C and conversion rate to PrP^Sc after infection with RML prions

Reaction rates	PrP isoforms		
	PrP^C	PrP^Sc	rPrP^Sc
	ng/d	ng/d	ng/d
Rate of expression (r_E)	707.3		
Rate of accumulation (r_A)		8.1	0.8
Rate of clearance (r_{CL})		2.7	0.3
Rate of conversion (r_C)		10.8	1.0

The following formulas were used: (a) rate of expression $r_E = ([PrP^C]/2)/t_{1/2}$; (b) rates of accumulation, PrP^Sc: $r_A = -672 + (8.12 \times \text{time in days})$ (R = 0.99); rPrP^Sc: $r_A = -62 + (0.77 \times \text{time in days})$ (R = 0.99); (c) rate of clearance $r_{CL} = (r_A/2)/t_{1/2}$; (d) rate of conversion $r_C = r_A - r_{CL}$.

monoglycosylated and unglycosylated PrP^C bands in fractions 9 and 10 (versus the abundance of diglycosylated, monoglycosylated, and unglycosylated protein found in disease-free animals; Figure 3A). In the next experiment, we used gel analysis to examine the upper velocity gradient fractions (fractions 10, 9, and 8) from the 3 mouse-adapted scrapie prion strains. For this purpose, samples were normalized according to PrP immunoblot signal when electrophoresed alongside equivalent gradient fractions from uninfected control animals. Protein samples were examined with or without PNGaseF deglycosylation (Figure 3, B and C). Although low levels of proteinase K–resistant (PK-resistant) PrP^Sc (~8% of total rPrP^Sc and 2% of PrP^C) were detected in each strain/host combination in the upper fractions of velocity gradients (Figure 1 and Supplemental Figure 1), unexpectedly high amounts of the PrP C2 carboxyl-terminal fragment colocalized in the upper gradient fractions with protease-sensitive PrP^C (Figure 3, C and D). This is of interest because the C2 cleavage fragment is generally considered to be a rPrP^Sc product, not a PrP^C product (21). Furthermore, comparison with the untreated samples indicates that this C2 fragment is primarily in its unglycosylated form (Figure 3B).

Preclinical PrP^C downregulation in infected WT mice. As Sho downregulation occurs preclinically (10, 11), we next assessed a time course of WT mice challenged with RML prions or negative control inoculum. Levels of Sho and the different PrP species were analyzed, showing a coincident appearance of the disease-associated PrP C2 fragment and Sho reduction by 120 days after inoculation (dpi), a finding in line with previous reports (10) (Figure 4, A and B). Using velocity gradient centrifugation plus CDI analysis on the time course series, rPrP^Sc began to increase by day 30 and continued to accumulate throughout the disease course (Figure 5A), a trend that paralleled a determination of infectious titer by scrapie cell assay in L929 cells (Figure 4C). However, these data illustrated a downturn for the rate of PrP^Sc replication at 60 dpi (Figure 5A). A biphasic profile was seen for PrP^C in the infected mice, with a marked decrease beginning 60 dpi (Figure 5B), suggesting an inverse relationship to the aforementioned rPrP^Sc levels. This effect was even more noticeable, as it diverged from the slow rise in PrP^C measured in aging mock-inoculated controls (Figure 5B).

In the interval of 60 to 140 dpi, PrP^C levels in infected mice fell by over 40%, from 1,200 to 700 ng/ml. To ascertain whether the preclinical drop in PrP^C levels was merely attributable to depletion of PrP^C substrate to make new PrP^Sc, we fit the data deriv-

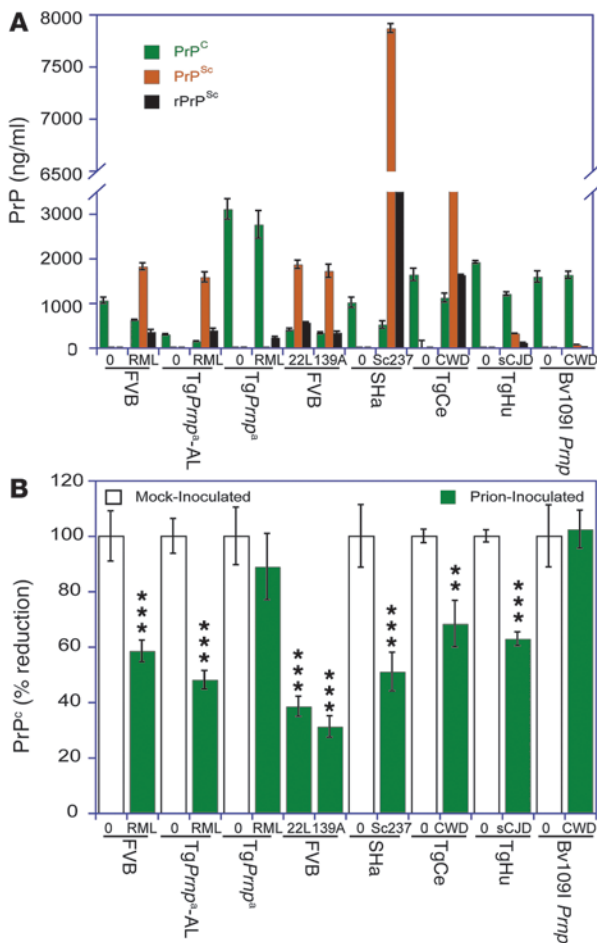**Figure 2**
PrP^C downregulation as a common feature of prion disease. (**A**) Concentration of PrP^C (green), total PrP^{Sc} (brown), and PK-resistant PrP^{Sc} (black) in brains of end-stage infected animals as follows: WT FVB mice challenged with RML, 22L, or 139A scrapie prions; RML-infected Tg*Prnp^a*-AL mice expressing 0.53 times endogenous PrP^C levels of WT mice; RML-infected Tg*Prnp^a* mice overexpressing PrP^C; Syrian hamsters (SHa) inoculated with Sc237 scrapie prions; TgCe "cervidized" mice inoculated with CWD prions; TgHu "humanized" mice challenged with human sCJD prions; and bank voles (Bv109I *Prnp*) inoculated with CWD prions. (**B**) Percentage reduction in PrP^C relative to uninfected animals for data represented in **A**. Healthy mock-infected controls (0; white columns) were compared to inoculated animals (green columns). The columns and error bars represent average ± SEM measured in 3 brains, each sample tested in duplicate or triplicate by CDI. ***$P < 0.001$, **$P < 0.01$, determined by ANOVA.

ing from CDI analyses of RML prion-infected animals with data obtained from our previous work on RML prion-infected bigenic mice (22). Specifically, the expression rate of PrP^C (r_E) was derived using the equation $r_E = ([PrP^C]/2)/t_{1/2}$, where the half-lives ($t_{1/2}$) for net brain PrP^{Sc} (i.e., sPrP^{Sc} plus rPrP^{Sc}) and brain PrP^C were determined to be 36 hours and 18 hours, respectively (see Table 1 and ref. 22). The accumulation rates (r_A) of PrP^{Sc} and rPrP^{Sc} were then obtained by linear fit of the data at 90 to 140 dpi with RML isolate: PrP^{Sc} $r_A = -672 + (8.12 \times$ time in days) (R = 0.99); rPrP^{Sc} $r_A = -62.4 + (0.77 \times$ time in days) (R = 0.99). Clearance rates (r_{CL}) of PrP^{Sc} and rPrP^{Sc} were calculated from the half-life of mouse

PrP^{Sc} determined previously (22) in RML prion-infected doxycycline-regulated bigenics and accumulation rates of PrP^{Sc} and rPrP^{Sc} obtained in this study: $r_{CL} = (r_A/2)/t_{1/2}$. Finally, the conversion rate (r_C) of PrP^C to PrP^{Sc} in the brain was determined from the accumulation rate of PrP^{Sc} corrected for clearance: $r_C = r_A - r_{CL}$. According to these calculations, the expression rate of PrP^C was estimated to be approximately 65-fold higher than the conversion rate to total PrP^{Sc} and approximately 700-fold higher than the conversion rate to rPrP^{Sc}, thus implying that depletion of PrP^C for the synthesis of PrP^{Sc} is a negligible factor in determining the drop in steady-state levels of PrP^C (i.e., downregulation). Also, speaking to degenerative changes, PrP^C downregulation preceded alterations in the neuron marker NeuN, and we observed no changes in the GPI-linked Thy1.2 glycoprotein associated with caveolae (ref. 23 and Supplemental Figure 7).

PrP^C downregulation in models with different levels of starting PrP^C. Although prior studies have defined a profound effect of PrP^C levels in healthy mice on disease incubation times subsequent to inoculation (24, 25), a downregulation effect was never considered in the interpretation of these studies. Consequently, we investigated prion infections in mice underexpressing or overexpressing PrP^C.

To evaluate underexpression, we conducted a time course for RML prion-infected FVB/N hemizygous knockout (*Prnp$^{0/+}$*) mice and controls inoculated with normal brain homogenate. Hemizygous *Prnp$^{0/+}$* mice are established as generating high levels of infectivity and PrP^{Sc} months before exhibiting symptoms of prion disease (26). To this effect, we observed that PrP^{Sc} began to accumulate in the brains of these animals between 60 and 100 dpi (Figure 5C). As in the case of WT animals, a parallel preclinical decrease in PrP^C levels and PrP^{Sc} replication rate was observed in infected hemizygotes beginning at 100 dpi (nearly 300 days before the expected time in which they succumb to disease; ref. 26), and both parameters continued dropping throughout the time course, reaching levels approximately 40% lower than those of the controls ($P < 0.001$) (Figure 5, C and D). This was accompanied by a gradual decrease in Sho throughout the duration of the time course (Figure 5E). While this cohort of animals has yet to reach disease end point, the effects of underexpression later in the disease course were explored using the Tg*Prnp^a*-AL mouse line made on a *Prnp$^{0/0}$* background and expressing 53% of WT levels of PrP^C-A (Supplemental Figure 8). When measured in RML prion-infected mice at disease end point (400–430 dpi), the absolute PrP^C levels in ng/ml lysate were downregulated to the lowest in our survey (Figure 2).

Uninfected adult Tg*Prnp^a* mice overexpress 6 to 7 times PrP^C levels of WT mice and have incubation periods of 60 to 80 dpi (20, 27). By CDI, the highest PrP^C levels in uninfected Tg*Prnp^a* mice (C57BL6 background) were approximately 3 times those seen in WT FVB/N mice (Figure 2A). Infected Tg*Prnp^a* animals and normal brain homogenate inoculated controls were investigated in a time course series (Supplemental Figure 9, A–C). Tg*Prnp^a* animals were also discovered to exhibit a biphasic PrP^C profile, albeit with a smaller effect size (11%, measured between 45 and 60 dpi), that was not significant due to the interindividual variability (±12%) (Supplemental Figure 9B). Nonetheless, a downturn in rPrP^{Sc} replication rate was noted when comparing the same 2 time points (Supplemental Figure 9A), offering an analogous trend to the effect noted in WT and hemizygous *Prnp$^{0/+}$* mice (Figure 5, A and C). Like PrP^C, Sho levels were affected little during the disease process in these mice (Supplemental Figure 9C).
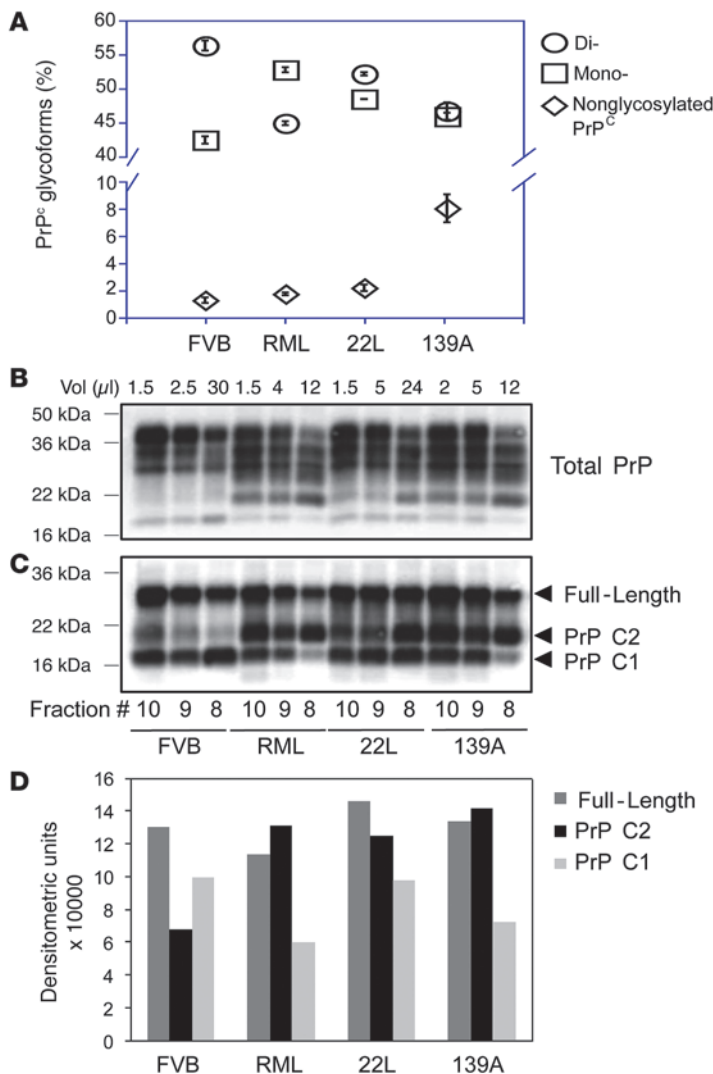
Figure 3
Glycosylation and fragmentation of PrP^C altered by prion infection. (**A**) PrP^C glycoform ratios for protein in gradient fractions 10, 9, and 8 for WT mouse brain and brains of mice with end-stage disease caused by RML, 22L, or 139A scrapie prions were determined for Western blots represented in Figure 1A and Supplemental Figure 1A. Diglycosylated, monoglycosylated, and unglycosylated forms are shown by circles, squares, and diamonds, respectively. The columns and error bars represent average ± SEM measured in 3 brains, each sample tested in duplicate or triplicate by CDI. The same gradient fractions for the 3 mouse-adapted scrapie samples were normalized by immunoblot signal and compared to uninfected controls ("healthy") in blot analyses (**B**) before and (**C**) after PNGaseF deglycosylation. (**D**) Densitometry was performed to evaluate the net levels of full-length PrP and its C-terminal fragments (PrP C1 and PrP C2), as shown in **C**.

These data suggest that notable effect sizes for PrP^C downregulation are associated with long prion incubation times and vice versa. By plotting the incubation times of RML prions in these 3 hosts (all with the same *Prnp^a* genotype but expressing different levels of PrP^C) versus terminal concentrations of PrP^C and rPrP^{Sc}, we found that prion infection caused a highly significant shift in the slope of the linear regression between incubation time of the disease and end point levels of PrP^C (Figure 6A and ref. 4). This shift in slope reflects a correlation for PrP^C downregulation in the infected animals, with the largest difference in the data with or without infection occurring in the Tg*Prnp^a*-AL animals. A correlation was also apparent after plotting incubation time and the ratio between end point PrP^C and rPrP^{Sc} (Figure 6B). Cumulatively, downregulation of PrP^C was linked to the low expression levels of PrP^C and high levels of the accumulated rPrP^{Sc} at disease end stage and is associated with prolonged incubation time (R = 0.99, *P* < 0.001). We next applied a similar plotting scheme to the spectrum of prion strains and disease models inoculated in our experiments. We found that this effect is broadly applicable despite independent variables that included 4 different *Prnp* genotypes, different starting PrP^C levels, and 6 different strains of prions (Figure 6C; R = 0.77, *P* < 0.05).

Assessing PrP^C downregulation in bank voles. Bank vole–adapted CWD prions produce the fastest prion disease in a naturally occurring animal host and hence are important in assessing the interplay between prion replication and disease pathogenesis (28). A time course series of samples was again investigated (Supplemental Figure 9, D–F). Unlike the other prion-infected specimens examined, PrP^{Sc} generated in the bank vole was primarily composed of oligomers sensitive to PK digestion (Supplemental Figure 6), a form that has been described as the most infectious PrP species (29). In this disease model, neither PrP^C nor Sho levels differed between CWD- and mock-inoculated animals despite the low but continuous accumulation of rPrP^{Sc} observed in the brain 20 dpi (Supplemental Figure 9, E and F). However, a biphasic replication profile was again noted for rPrP^{Sc}, with a maximum increase from 20 to 25 dpi and steady decline during the final 5 days of disease (Supplemental Figure 9D). The short incubation period in CWD-infected bank voles may be related to the ability to rapidly generate PK-sensitive oligomers in the absence of Sho downregulation (Supplemental Figure 6 and Supplemental Figure 9F) (and PrP^C downregulation) that may be typically triggered by rPrP^{Sc} (10, 11).
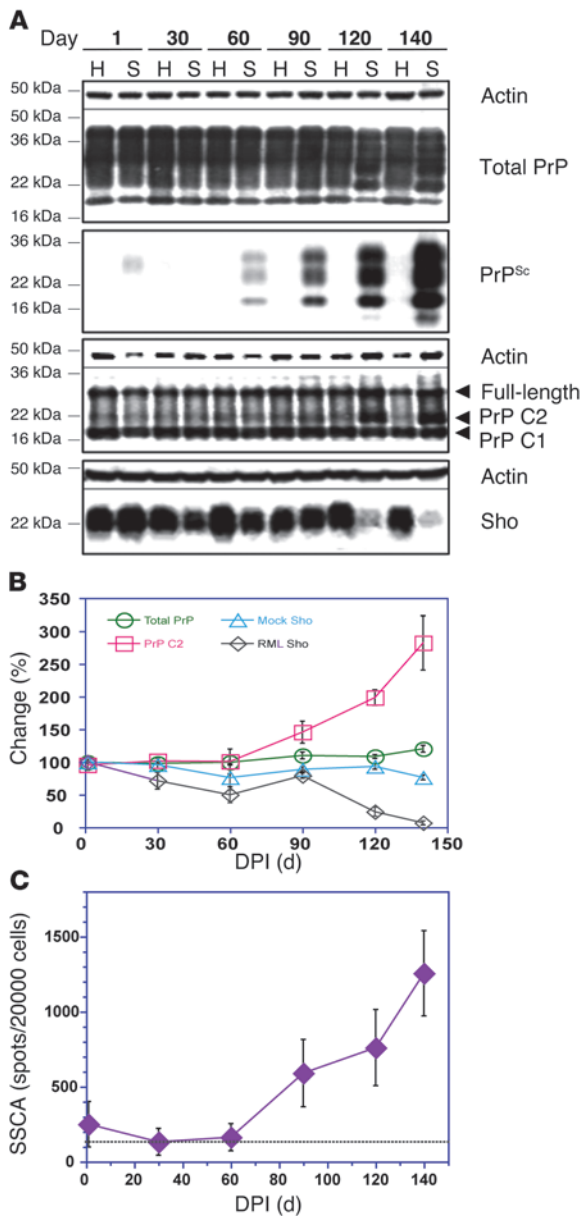
Figure 4
Time course analysis of control and pathogenesis-related proteins in infected mouse brain (RML isolate). (**A**) Samples were analyzed by Western blot of homogenates from sagittally bisected brain. "H" and "S" designate healthy and sick (prion-infected) animals. Antibody probes include the following: untreated samples for total PrP, PK-digested samples for PrPSc, fragmentation products (C2, C1) for PrP shown subsequent to PNGase F digestion, and Sho. (**B**) Percentage change for PrP C2 fragment, total PrP, and Sho (RML Sho) is presented for the time course in infected animals. Baseline Sho levels from mock-infected animals (mock Sho) are also shown. Values were determined from densitometric analysis of blots in **A**. (**C**) SSCA performed in L929 cells to estimate time course of infectivity; the dotted line represents assay threshold. The columns and error bars represent average ± SEM measured in 3 brains, each sample tested in duplicate or triplicate by CDI.

PrP^C downregulation in cultured cells. We wanted to investigate whether preclinical PrP^C downregulation observed in vivo is associated with PrP^{Sc} accumulation (as previously demonstrated for Sho; refs. 10, 11) or is a side effect of neurodegenerative change. We explored this possibility using monocultures of cells that lack pathological signs upon prion infection (30). First, we compared N2a neuroblastoma expressing mouse PrP^C-A (N2a) (31) and rabbit RK13-Gag cells expressing elk PrP^C (RK13 Elk21) (32) chronically infected with RML prions or elk CWD prions, respectively. In both cases, corresponding PrP^C reductions were approximately 35% and 55% compared with noninfected controls (Figure 7, A and B). Next, to parallel in vivo time course experiments in the brain, we carried out de novo infections, monitoring RK13 cells stably expressing either mouse *Prnp^a* or *Prnp^b* for 5 weeks after treatment with RML-infected brain homogenate (Figure 7 and Supplemental Figure 10). Similar infections with mouse-adapted scrapie prions in vivo have demonstrated drastically different susceptibilities for mice with these genotypes, where mice with the *Prnp^a* genotype exhibit significantly shorter prion incubation periods than those with the *Prnp^b* genotype (33). In parallel, expression of PrP^C-A made RK13 cells highly susceptible to RML prion infection (Figure 7, C and D; Supplemental Figure 10A; and refs. 25, 34). In comparison to mock-inoculated cells, propagation of PrP^{Sc} resulted in a decrease in PrP^C until 21 dpi, with levels then recovering to control levels by 35 dpi (Figure 7D). The converted rPrP^{Sc} represented 0.3%–0.5% of homologous PrP^C expressed in these cells. In contrast, RK13 cells expressing PrP^C-B were resistant to infection (Figure 7C and Supplemental Figure 10B). Since downregulation did not occur in cells expressing PrP^C-B (Supplemental Figure 10C), the effect seen in *Prnp^a*-expressing cells is not a response against administration of the brain homogenate but is instead a consequence of a productive infection. Cumulatively, the cell data provide evidence that neither neuronal loss accompanying prion disease nor conversion of PrP^C to PrP^{Sc} can account, per se, for the PrP^C downregulatory effect.

Impact of PrP^C downregulation on prion replication rate. Since prion replication rate decreased in tandem with PrP^C downregulation in our time course studies, we investigated the relationship between these 2 events by simulating rPrP^{Sc} propagation during the prion infection process in vitro with PMCA (14, 35). First, we examined PMCA products for experiments seeded with increasing amounts of 139A prions in a constant amount of PrP^C; here, PrP^{Sc} amplification was found to be a saturable component at PrP^{Sc} seed concentrations of ≥1 ng/ml (Supplemental Figure 11A). This may be analogous to the decreased PrP^{Sc} replication rate at end point prion disease in the absence of PrP^C downregulation, as described above for Tg*Prnp^a* mice and bank voles. In experiments holding the RML PrP^{Sc} "seed" constant, dropping PrP^C input in the range of 1,100 to 1,400 ng/ml (similar to the change in PrP^C in early versus end stage disease in WT mice; Figure 5B) had a marked impact upon replication rate (Supplemental Figure 11B), thus indicating that PrP^C is a limiting factor, as previously reported (36). To simulate conditions more precisely over the course of prion infection, RML PrP^{Sc} seeds and PrP^C substrate were inversely titrated to test the impact on amplification. At PrP^C concentrations below approximately 350 ng/ml and PrP^{Sc} seed concentrations of ≥1 ng/ml PrP^{Sc}, the replication rate was held below an amplification index of 20-fold, apparently due to saturation with an abundance of PrP^{Sc} (Figure 7E). However, at higher ng/ml values of PrP^C, these two traces diverge and hence are associated with a concomitant increase in replication
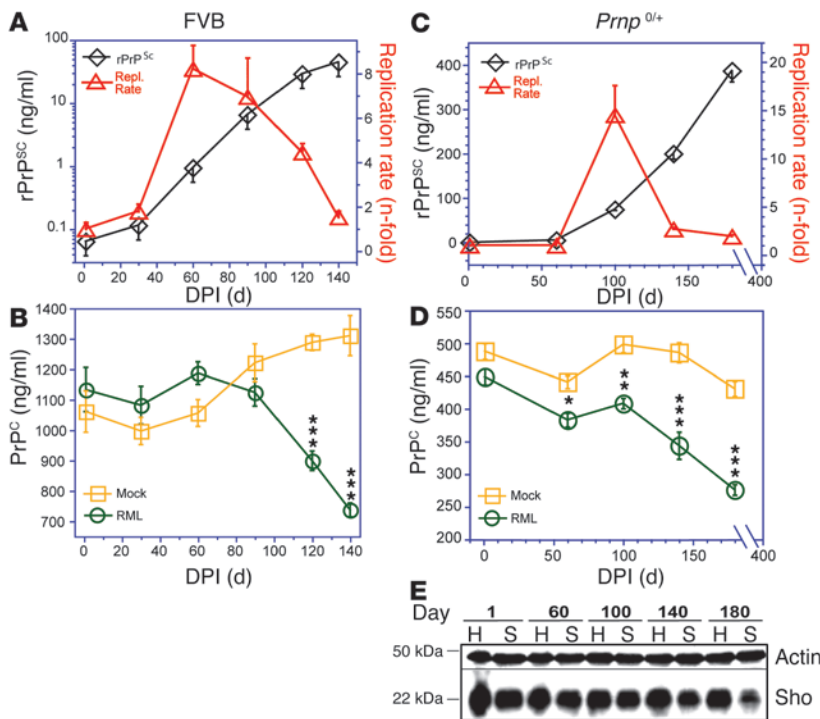
Figure 5
Preclinical drop in PrP^C levels, Sho levels, and PrP^{Sc} replication rate. Time courses were performed for (**A** and **B**) WT FVB mice and (**C**–**E**) hemizygous *Prnp$^{0/+}$* mice infected with RML prions and compared to mock-inoculated controls. (**A** and **C**) CDI analysis of brain material was used to evaluate rPrP^{Sc} levels (black diamonds) and to calculate the rPrP^{Sc} replication rate (red triangles). (**B** and **D**) Corresponding CDI data for brain PrP^C for mice in **A** and **C**: yellow squares represent control mice and green circles represent RML-infected mice. (**E**) Western blot analysis was used to compare Sho levels over time in hemizygous *Prnp$^{0/+}$* mice either inoculated with RML prions ("S" for sick) or mock-inoculated ("H" for healthy) (see analogous Sho data for WT in Figure 4A). The data points and error bars represent average ± SEM measured in 3 brains, each tested in duplicate or triplicate by CDI. ***$P < 0.001$, **$P < 0.01$, *$P < 0.05$, determined by ANOVA.

rate, up to a factor of 110-fold (Figure 7E). These inverse titration experiments were extended to include 139A mouse-adapted prions (Supplemental Figure 11C), human sCJD prions (Supplemental Figure 11D), and Syrian hamster Sc237 prions (Supplemental Figure 11E). In every case, a uniform biphasic response was observed for each set of PMCA reactions, in which the most efficient amplification occurred in conditions paralleling an early stage of infection, with a low concentration of PrP^{Sc} and a high concentration of PrP^C. Therefore, our PMCA data indicate that rising PrP^{Sc} levels and falling PrP^C levels will converge to suppress prion replication. Furthermore, these results point to an affect of PrP^C downregulation beginning halfway through the incubation time interval in WT mice (Figure 5B).

Discussion

Two unaddressed factors for prion infection are their long incubation periods and observed discrepancies between PrP^{Sc} levels and clinical disease (4, 37). However, using capture and conformational antibodies to inventory the different PrP species in the brain (i.e., rPrP^{Sc}, sPrP^{Sc}, and PrP^C), we have defined a new variable in disease pathogenesis, namely preclinical downregulation of PrP^C. This downregulation does not emanate from changes in PrP mRNA abundance (12, 13, 38).

PrP^C is indisputably required for the creation of PrP^{Sc} (2, 3, 24), but depletion by the law of mass action (i.e., a finite pool of PrP^C "substrate" being consumed by a thermodynamically favorable conversion to PrP^{Sc}) is implausible as the rate of PrP^C synthesis in the brain outstrips the rate of formation of total PrP^{Sc} and rPrP^{Sc} by about 1 and 2 orders of magnitude, respectively (Table 1). It is also known from metabolic labeling of chronically infected cell cultures that only approximately 1% to 5% of PrP^C converts into PrP^{Sc} (39, 40). Declining levels of PrP^C in the course of protracted prion infections were in most instances shadowed by a drop in

endogenous mouse Sho (refs. 10, 11; Figures 1, 4, and 5; and Supplemental Figures 1 and 9), a cousin of PrP^C that does not modulate creation of PrP^{Sc} and is not converted to a protease-resistant isoform (41). Depletion of PrP^C as a simple consequence of synaptic damage or neuronal cell death is unlikely, because PrP^C downregulation occurred nearly 300 days before clinical disease in hemizygous *Prnp$^{0/+}$* mice and was absent in certain rapid models with an abundance of vacuolation at end stage disease (i.e., Tg*Prnp^a* mice and bank voles; Figure 5D and Supplemental Figure 9, B and E). Moreover, PrP^C downregulation was detected in cell culture models that are undergoing mitosis and have no synapses (Figure 7, A–D). The recovery phase noted 2 weeks later in these de novo infections may reflect selection pressures operating within the cultures of infected but mitotically active cells. From these observations, we suggest first that a host protective response is operating at the level of a cellular biological mechanism, presumably a form of proteostasis. Second, we suggest this response is triggered by the presence of rPrP^{Sc} and reduces net levels of PrP^C and Sho by a "bystander" effect (Figure 8 and refs. 8, 10, 11). The reduction in net PrP^C levels defined by our experiments stands in apparent contrast to a redistribution effect in persistently infected cells, in which cell surface PrP is reduced and immunohistochemical signal in a *trans*-Golgi network subcompartment is increased (42).

Thus far, we have not identified the tell-tale signs of a single canonical proteostatic pathway, such as eIF-2αP (translation axis of the unfolded protein response) (43), LC3-II (autophagy), or ubiquitin (proteasome system) (Supplemental Figure 7). The largely parallel downregulation of PrP^C and Sho indicates remodeling of a membrane microdomain that includes these proteins but does not include Thy-1.2 (Supplemental Figure 7A). However, the changes in the quality of PrP^C (less diglycosylated, preponderance of C2 fragment) contrast with an across-the-board
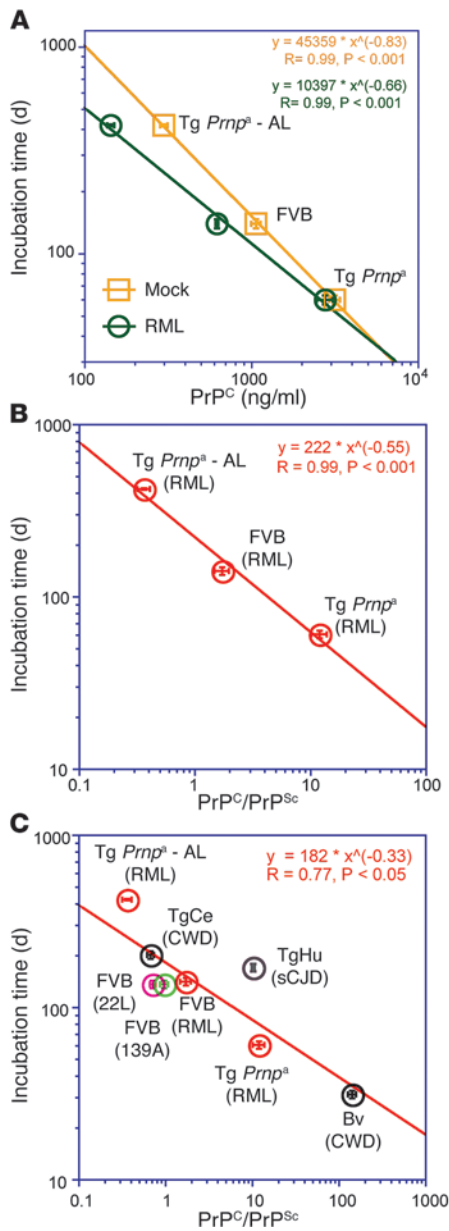
Figure 6
Relationships between end point PrP^C/PrP^{Sc} ratios and prion incubation period. (**A**) Residual PrP^C plotted against incubation time for the RML prion isolate in 3 mouse genotypes expressing different amounts of the PrP-A protein. Data points for mock-inoculated controls (yellow line) and end-stage RML prion-infected animals (green line) represent, from left to right, Tg*Prnp^a*-AL, WT FVB, and Tg*Prnp^a* mice all infected with the RML prion isolate. (**B**) Ratios of residual PrP^C/residual PrP^{Sc} at disease end point plotted against incubation time for mouse genotypes presented in **A**. (**C**) Cumulative data for residual PrP^C/residual PrP^{Sc} at disease end point for 8 prion strain/host genotype combinations.

change that might be expected for a hypotheses of mass action depletion or cell death and were unexpected. The C2 aspect is especially notable as Watts and colleagues recently argued that Sho is degraded via an endocytic pathway that requires it to be physically trafficked with PrP^{Sc} (10). A component of this argu-

ment was the inverse correlation between Sho levels and the PrP C2 proteolytic fragment (10), with the latter hypothesized as a stable intermediate in the lysosomal degradation of PrP^{Sc} (44, 45). However, we have shown that models for other neurodegenerative diseases with activated lysosomes lack downregulation of Sho (11). Although our analyses of total cell lysates reaffirm a correlation between the reduction in Sho levels and the appearance of the protease-resistant PrP C2 proteolytic fragment toward disease end point (Figure 4A), our analyses of fractionated cell lysates demonstrated a surprising abundance of C2 colocalized in the upper gradient fractions. This suggests that protease-resistant C2 found toward disease end point derives from a protease-sensitive, and thus partly PrP^C-like, precursor molecule. While the identity of an endoproteolytic "C2 PrPase" (like C1 PrPase; ref. 46) is unknown, progress in this area will help us to understand early events in PrP^{Sc} synthesis and early host responses. Another area of interest will be whether other parameters, such as a limited concentration of a cofactor (e.g., phosphatidylethanolamine; refs. 47, 48), can also contribute to a curtailment in the exponential phase for prion replication.

Prior studies have invoked a hypothetical toxic subform of PrP to explain the beneficial effects of a genetic reduction in PrP^C levels that cause a delay between plateauing infectivity levels and the onset of clinical symptoms (4, 49). Here, an alternative explanation emerges from the observed changes with time in PrP isoforms. We show that the ratio between residual PrP^C seen in end-stage disease and the amount of PrP^{Sc} is clearly correlated with the time lag to disease onset, and present experimental manipulations strongly suggest that this ratio in fact determines time lag. Within this formula, when PrP^{Sc} and infectivity reach a plateau (4), the extent of PrP^C downregulation becomes the key variable. The difference between quickly and slowly evolving disease can be seen clearly in the different slopes shown in Figure 6A, and we therefore suggest that the slowly evolving infection of the central nervous system (most typical of natural prion disease) can be seen to arise from downregulation of the very same substrate required both for de novo PrP^{Sc} synthesis and for pathogenic signaling, as defined by grafting experiments (50) and by use of regulated PrP^C expression (49). Interestingly, while the need to hypothesize a toxic subform of PrP^{Sc} may be less urgent, PrP^C downregulation can be reconciled with the measurements that led some to posit a 2-phase model for prion disease (4) or a form of substrate depletion predicted from analysis of prion disease kinetics (51). Cumulatively, our data show that slowly evolving pathogenesis of preclinical disease is caused by depletion of the PrP^C substrate that is required for PrP^{Sc} synthesis and toxic signaling. We infer that the natural phenomenon of PrP^C downregulation is partially effective in holding prion disease in check in WT animals. Drugs that enhance this protective response to further reduce PrP^C may have a potent beneficial effect in treating prion disease.

Methods

Mouse lines, prion bioassays, and brain homogenates. WT mice, hemizygous *Prnp$^{0/+}$* mice, Tg*Prnp^a*-AL mice expressing 53% WT levels of PrP-A and made by standard procedures using the PrP half-genomic construct (ref. 20 and see Supplemental Figure 8), Tg*Prnp^a* mice maintained as homozygous stock (20), humanized Tg40 mice (HuPrP-129M) (19), and cervidized Tg33 mice (Deer PrP-96G) (18) were used in this study. Mice were inoculated at 3 to 6 weeks of age with 30 to 50 μl 1% w/v brain homogenate containing mouse-adapted scrapie (RML, 22L, or 139A),
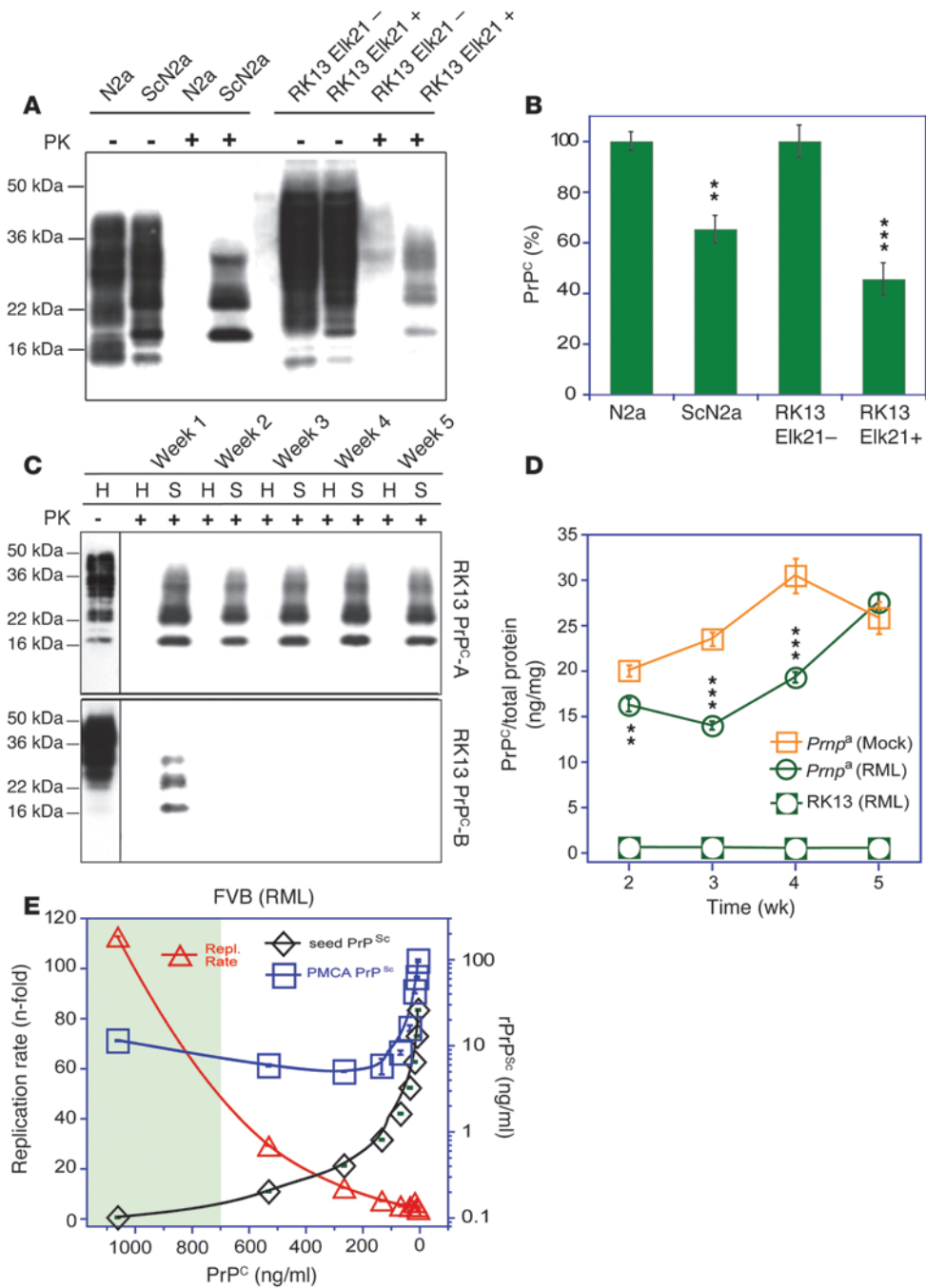
Figure 7

PrP^C downregulation examined in cell culture models and by PMCA. (**A**) Western blot analysis was used to show PK sensitivity of cell lysates derived from uninfected N2a, ScN2a (chronically infected with RML scrapie prions), uninfected RK13 Elk21⁻, and RKE21⁺ (chronically infected with elk CWD prions). (**B**) CDI was used to evaluate the relative downregulation of PrP^C in these cell lines. (**C**) Western blot analysis was used to show PK sensitivity of RK13 cells stably expressing either PrP^C-A or PrP^C-B following exposure to RML prions. (**D**) CDI was applied to quantify the PrP^C levels in RK13 cells stably expressing PrP^C-A following treatment with healthy (square) or RML-infected brain material (circle). Normal RK13 cells treated with RML-infected brain material (box with circle) were used as a control. (**E**) PrP^{Sc} replication rate was evaluated using double PMCA titrations to assess the effect of decreasing PrP^C input and titrated amounts of PrP^{Sc} "seed" from mouse-adapted RML prions. The columns and data points and error bars represent average ± SEM measured in triplicate. **$P < 0.01$, ***$P < 0.001$, determined by ANOVA.
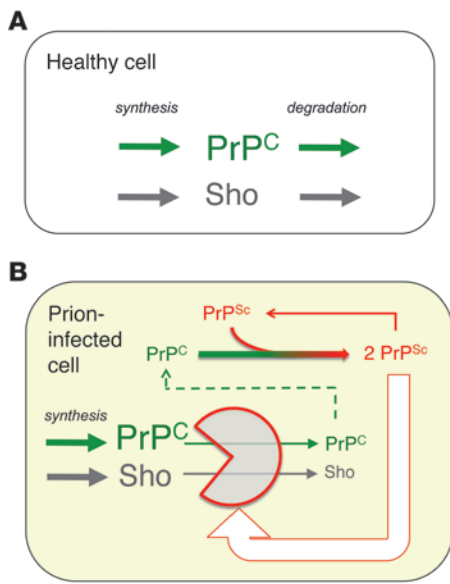
Figure 8
Summary of PrP^C and Sho downregulation in a prion-infected cell by an unidentified degradation pathway. (**A**) In a healthy cell, the balance of synthesis rate and degradation rate establish the steady-state level of PrP^C and Sho. (**B**) We assert that prion-infected cells are characterized by two processes. The first is the well-known biosynthetic conversion of PrP^C to PrP^{Sc} (top part of cell). We hypothesize a second process (bottom part of the cell) in which the accumulation of PrP^{Sc} triggers (open arrow) a proteostatic degradative response (Pac-Man shape). This in turn reduces the steady-state concentrations of PrP^C and Sho (indicated by smaller text) by a "bystander effect." Reduced PrP^C will have an impact on PrP^{Sc} synthesis (dotted green line). An additional effect of PrP^C reduction may be to attenuate toxic signaling (see the Discussion), but this concept is omitted from the diagram for the sake of simplicity.

MM1 sCJD (homozygous for methionine in polymorphic codon 129 of the *PRNP* gene and 21-kDa fragment [type 1] of unglycosylated rPrP^{Sc} on Western blots after PK treatment), or white-tailed deer CWD prions. Bank voles (Bv109I *Prnp*) were inoculated at 8 weeks of age with 20 μl brain homogenate containing bank vole–adapted elk CWD prions. For analysis, 10% w/v homogenate was made in PBS by serial passing through needles.

Sucrose gradient and CDI. Sucrose gradient and CDI were performed as previously described (14). Briefly, the 400-μl aliquots of 10% brain homogenate in PBS, pH 7.4, containing 2% Sarkosyl were clarified by centrifugation at 500 *g* for 5 minutes and carefully layered onto the top of the 10% to 45% sucrose gradient prepared in PBS, pH 7.4, containing 1% Sarkosyl. Ultracentrifugation was performed at 237,000 *g* for 73 minutes at 5°C in an Optima TL ultracentrifuge (Beckman) equipped with a Beckman SW 55 Ti rotor. After the centrifugation, fractions were collected from the bottom of the tube.

The CDI assay was similar to previous descriptions (15, 52), albeit with several modifications. First, we used white Lumitrac 600 High-Binding Plates (E&K Scientific) coated with mAb 8H4 (epitope 175–185) (53) in 200 mM NaH$_2$PO$_4$ containing 0.03% (w/v) NaN$_3$, pH 7.5. Second, 20-μl aliquots from each fraction containing 0.007% (v/v) of Patent Blue V (Sigma-Aldrich) were directly loaded into wells of white strip plates pre-filled with 200 of Assay Buffer (Perkin Elmer). Finally, the captured PrP was detected by a europium-conjugated (5) anti-PrP mAb 3F4 (epitope 108–112) (54) or Europium-labeled mAb 12B2 (epitope 88–92) (16), and the time-resolved fluorescence (TRF) signals were measured by the multimode microplate reader PHERAstar Plus (BMG LabTech). The recombinant human PrP(90–231, 129M) and PrP(23–231, 129M) used as a calibrant in the CDI were a gift from Witold Surewicz (Department of Physiology and Biophysics, Case Western Reserve University), and preparation and purification have been described previously (55). The initial concentration of recombinant human PrP(23–231, 129M) and PrP(90–231, 129M) was calculated from absorbance at 280 nm and molar extinction coefficient 56,650 M^{-1}cm^{-1} and 21,640 M^{-1}cm^{-1}, respectively. The purified recombinant proteins were dissolved in 4 M GdnHCl and 50% Stabilcoat (SurModics) and stored at –80 °C. The concentration of PrP was calculated from the CDI signal of denatured samples using a calibration curve prepared with either recombinant PrP(23–231, 129M) for samples containing full-length PrP^{Sc} or recombinant PrP(90–231, 129M) for samples containing truncated rPrP^{Sc} [PrP(27–30)] after PK treatment.

The calibration and validation aspect of CDI has been reported on extensively by us and others (5, 14, 15, 56–62). Briefly, the PK-untreated sample containing PrP is divided into native and denatured aliquot, and the later is denatured with 4 M Gdn HCl for 5 minutes at 80°C. Using Eu-labeled mAb 3F4 or 12B2 for detection, the TRF signal of native sample corresponds to the epitope 107–112 that is exposed in α-helical PrP^C and hidden in PrP^{Sc} and is proportional to the concentration of PrP^C (5). The signal of denatured aliquot corresponds to the total PrP in a sample, and the concentration of PrP^{Sc} is then calculated according formula: [PrP^{Sc}] = [PrP$_D$] – [PrP$_N$], where *D* stands for denatured aliquot and *N* stands for native aliquot. Next, the concentration of rPrP^{Sc} is calculated in samples subjected to PK treatment followed by complete denaturation using PrP(90–231, 129M) calibration curve. The concentration of sPrP^{Sc} is calculated according formula: [sPrP^{Sc}] = [PrP^{Sc}] – [rPrP^{Sc}]. The separate calibration for the PK-treated and untreated sample is critical for correct results due to the approximately 3.5-fold lower affinity of mAb 3F4 with denatured full-length human PrP(23–231, 129M) compared to PrP(90–231, 129M) (14, 56).

SSCA. SSCA was performed as described previously (63), with some modifications. Briefly, L929 cells were exposed to varying concentrations of brain homogenates (0.1–0.0001% w/v) for 5 days in 96-well culture plates. The cells were passaged 3 times (1:4 and 1:7), with 20,000 cells collected at the third passage and loaded on to Multiscreen$_{HTS}$ IP 96-well, 0.45-μM filter plates (Millipore). The cells were first subjected to PK digestion (5 μg/ml) followed by denaturation using 3 M guanidine thiocyanate. The Elispot reaction was performed using a mouse anti-PrP antibody (SAF83, 1:1,000) and a goat anti-mouse alkaline phosphatase–conjugated secondary antibody (1:5,000). The plates were developed using BCIP/NBT and analyzed using an Autoimmun Diagnostika GmbH Elispot plate reader (ELR07).

PMCA. Sonication-driven PMCA was performed as described previously (14, 64) with the following modifications. The PrP^{Sc} was replicated using brains of homologous species or Tg mice expressing homologous PrP^C (14). Brain homogenates from prion-infected animals were diluted as described in the specific experiments to attain final 10% brain homogenate, and 60 μl was transferred into 0.2-ml PCR tubes equipped with 2.38-mm diameter PTFE ball (K-mac Plastics). The buffer in all PMCA reactions was PBS, pH 7.4, containing final 1% Triton X-100, 500 mM NaCl, 0.1% Sarkosyl, and 1 mM of an antioxidant α-Tocopherol. Tubes were positioned on an adaptor placed on the plate holder of a microsonicator (Misonix Model 3000)

and programmed to perform cycles of 60-minute incubation at 35°C, followed by a 30-second pulse of sonication set at 80% power. Samples were incubated, without shaking, and immersed in the water of the sonicator bath for 48 cycles. The 30 μl of the amplified materials was transferred to the next tube, which was prefilled with 30 μl substrate brain homogenate for the next round, and the remaining 30-μl aliquot was analyzed with CDI and Western blot analysis. The amplification index was calculated in each round using the following formula: [PMCA rPrP^{Sc}]/[seed rPrP^{Sc}].

Cell culture and infection with prions. All RK13- and N2a-based cell lines were maintained in Dulbecco's Modified Eagle's Medium (Invitrogen) containing 10% fetal bovine serum and 1% penicillin-streptomycin at 37°C with 5% CO$_2$. To obtain RK13 cell lines stably expressing mouse *Prnp^a* and *Prnp^b*, RK13 cells were transfected with 1 to 5 μg of specified clones in pBud.GFP (65) at approximately 90% confluence with the Lipofectamine Plus reagent (Invitrogen) according to the manufacturer's specifications and selected in media supplemented with 1 mg/ml Zeocin. Prion infections were conducted under identical environmental conditions in 12-well plates containing Opti-Minimal Essential Medium supplemented with 25 μl 10% RML prion-infected or control brain homogenate as previously described (66).

Western blotting. 20–60 μg protein of each BCA-quantified (Pierce) sample was (a) deglycosylated overnight at 37°C with 250 to 500 U PNGaseF (New England Biolabs) and resuspended in gel-loading buffer (0.6 M Tris, pH 6.8; 2% SDS; 7.5% glycerol; 0.005% bromophenol blue; 2.5% β-mercaptoethanol); (b) digested with 100 μg/ml PK for 1 hour at 37°C, inactivated with 1 mM phenylmethylsulfonylfluoride, and resuspended in gel-loading buffer; or (c) directly mixed with gel-loading buffer. Each was boiled for approximately 10 minutes and electrophoresed through 14% Tris–Glycine SDS-PAGE gels. Proteins were transferred onto a PVDF (Immobilon-FL, Millipore) membrane. Blots were incubated with anti-Sho 06rSh1, anti-PrP SHA31 (Medicorp Inc.), anti-PrP mAb 12B2 (16), anti-PrP mAbSAF83 (Cayman), anti-PrP mAb 2D6 (a generous gift from H. Rezai; ref. 67), anti-Thy1.2 (Abcam), anti-PSD-95 (Millipore), anti-NeuN (Millipore), anti-LC3 (Millipore), anti-Ubiquitin (Santa Cruz), and anti–Phospho-eIF2α (Cell Signaling Technology). ECL Plus reagents (Amersham Pharmacia) were used for visualization by exposure of blots to film or by scanning with an ImageQuant 300 (GE Healthcare). In some instances PNGaseF (NE Biolabs) was used per the manufacturer's recommendations prior to blot analysis, and where appropriate, blots were reprobed with anti-actin primary antibody (Sigma-Aldrich) and anti-rabbit IgG secondary antibody conjugated to horseradish peroxidase. ImageJ software was utilized for densitometry analysis of the images (68).

Statistics. All the statistical analyses were performed using SPSS 19 software (SPSS Inc.), and P values were calculated using Anova. P values of less than 0.05 were considered significant and are specified in the legend for each figure.

Study approval. All protocols and experiments were approved by the IACUC of the Case Western Reserve University and University of Alberta.

Address correspondence to: David Westaway, University of Alberta, Centre for Prions and Protein Folding Diseases, 204 Brain and Aging Research Building, Edmonton, Alberta, Canada. Phone: 780.492.9024; Fax: 780.492.9352; E-mail: david.westaway@ualberta.ca. Or to: Jiri G. Safar, Case Western Reserve University, 11100 Euclid Ave., Cleveland, Ohio 44106, USA. Phone: 216.368.4609; Fax: 216.368.4090; E-mail: jiri.safar@case.edu.

1. Collinge J, et al. A clinical study of kuru patients with long incubation periods at the end of the epidemic in Papua New Guinea. *Philos Trans R Soc Lond B Biol Sci*. 2008;363(1510):3725–3739.
2. Wang F, Wang X, Yuan CG, Ma J. Generating a prion with bacterially expressed recombinant prion protein. *Science*. 2010;327(5969):1132–1135.
3. Büeler H, et al. Mice devoid of PrP are resistant to scrapie. *Cell*. 1993;73(7):1339–1347.
4. Sandberg MK, Al-Doujaily H, Sharps B, Clarke AR, Collinge J. Prion propagation and toxicity in vivo occur in two distinct mechanistic phases. *Nature*. 2011;470(7335):540–542.
5. Safar J, et al. Eight prion strains have PrPSc molecules with different conformations. *Nat Med*. 1998; 4(10):1157–1165.
6. Premzl M, Sangiorgio L, Strumbo B, Marshall Graves JA, Simonic T, Gready JE. Shadoo, a new protein highly conserved from fish to mammals and with similarity to prion protein. *Gene*. 2003; 314:89–102.
7. Watts JC, et al. The CNS glycoprotein Shadoo has PrP(C)-like protective properties and displays reduced levels in prion infections. *EMBO J*. 2007; 26(17):4038–4050.
8. Watts JC, et al. Interactome analyses identify ties of PrP and its mammalian paralogs to oligomannosidic N-glycans and endoplasmic reticulum–derived chaperones. *PLoS Pathog*. 2009;5(10):e1000608.
9. Miyazawa K, Manuelidis L. Agent-specific Shadoo responses in transmissible encephalopathies. *J Neuroimmune Pharmacol*. 2010;5(1):155–163.
10. Watts JC, et al. Protease-resistant prions selectively decrease shadoo protein. *PLoS Pathog*. 2011; 7(11):e1002382.
11. Westaway D, et al. Down-regulation of shadoo in prion infections traces a pre-clinical event inversely related to PrPSc accumulation. *PLoS Pathog*. 2011; 7(11):e1002391.
12. Chesebro B, et al. Identification of scrapie prion protein-specific mRNA in scrapie-infected and uninfected brain. *Nature*. 1985;315(6017):331–333.
13. Oesch B, et al. A cellular gene encodes scrapie PrP 27-30 protein. *Cell*. 1985;40(4):735–746.
14. Kim C, et al. Small protease sensitive oligomers of PrPSc in distinct human prions determine conversion rate of PrPC. *PLoS Pathog*. 2012;8(8):e1002835.
15. Safar JG, et al. Diagnosis of human prion disease. *Proc Natl Acad Sci U S A*. 2005;102(9):3501–3506.
16. Langeveld JPM, Jacobs JG, Erkens JHF, Bossers A. Rapid and discriminatory diagnosis of scrapie and BSE in retro-pharyngeal lymph nodes of sheep. *BMC Vet Res*. 2006;9:19.
17. Collinge J, Clarke AR. A general model of prion strains and their pathogenicity. *Science*. 2007; 318(5852):930–936.
18. Meade-White K, et al. Resistance to Chronic wasting disease in transgenic mice expressing a naturally occurring allelic variant of deer prion protein. *J Virol*. 2007;81(9):4533–4539.
19. Kong Q, et al. Chronic wasting disease of elk: Transmissibility to humans examined by transgenic mouse models. *J Neurosci*. 2005;25(35):7944–7949.
20. Fischer M, et al. Prion protein (PrP) with amino-proximal deletions restoring susceptibility of PrP knockout mice to scrapie. *EMBO J*. 1996; 15(6):1255–1264.
21. Chen SG, Teplow D, Parchi P, Gambetti P, Autilio-Gambetti L. Truncated forms of the human prion protein in normal brain and in prion diseases. *J Biol Chem*. 1995;270(32):19173–19180.
22. Safar JG, et al. Prion clearance in bigenic mice. *J Gen Virol*. 2005;86(pt 10):2913–2923.
23. Sheets ED, Lee GM, Simson R, Jacobson K. Transient confinement of a glycosylphosphatidylinositol-anchored protein in the plasma membrane. *Biochemistry*. 1997;36(41):12449–12458.
24. Prusiner SB, et al. Transgenetic studies implicate interactions between homologous PrP isoforms in scrapie prion replication. *Cell*. 1990;63(4):673–686.
25. Carlson GA, et al. Prion isolate specified allotypic interactions between the cellular and scrapie prion proteins in congenic and transgenic mice. *Proc Natl Acad Sci U S A*. 1994;91(12):5690–5694.
26. Büeler H, Raeber A, Sailer A, Fischer M, Aguzzi A, Weissmann C. High prion and PrPSc levels but delayed onset of disease in scrapie-inoculated mice heterozygous for a disrupted PrP gene. *Mol Med*. 1994;1(1):19–30.
27. Castro-Seoane R, et al. Plasmacytoid dendritic cells

sequester high prion titres at early stages of prion infection. *PLoS Pathog*. 2012;8(2):e1002538.

28. Di Bari MA, et al. Chronic wasting disease in bank voles: Characterisation of the shortest incubation time model for prion diseases. *PLoS Pathog*. 2013; 9(3):e1003219.

29. Silveira JR, et al. The most infectious prion protein particles. *Nature*. 2005;437(7056):257–261.

30. Vilette D. Cell models of prion infection. *Vet Res*. 2008; 39(4):10.

31. Klebe RJ, Ruddle FH. Neuroblastoma: cell culture analysis of a differentiating stem cell system. *J Cell Biol*. 1969;43(2):69a.

32. Bian J, Napier D, Khaychuck V, Angers R, Graham C, Telling G. Cell-based quantification of chronic wasting disease prions. *J Virol*. 2010;84(16):8322–8326.

33. Carlson GA, et al. Linkage of prion protein and scrapie incubation time genes. *Cell*. 1986;46(4):503–511.

34. Westaway D, Goodman PA, Mirenda CA, McKinley MP, Carlson GA, Prusiner SB. Distinct prion proteins in short and long scrapie incubation period mice. *Cell*. 1987;51(4):651–662.

35. Saborio GP, Permanne B, Soto C. Sensitive detection of pathological prion protein by cyclic amplification of protein misfolding. *Nature*. 2001; 411(6839):810–813.

36. Mays CE, Titlow W, Seward T, Telling GC, Ryou C. Enhancement of protein misfolding cyclic amplification by using concentrated cellular prion protein source. *Biochem Biophys Res Commun*. 2009; 388(2):306–310.

37. Bueler H, Raeber A, Sailer A, Fischer M, Aguzzi A, Weissmann C. High prion and PrPSc levels but delayed onset of disease in scrapie-inoculated mice heterozygous for a disrupted PrP gene. *Mol Med*. 1994; 1(1):19–30.

38. Aguib Y, Gilch S, Krammer C, Ertmer A, Groschup MH, Schatzl HM. Neuroendocrine cultured cells counteract persistent prion infection by down-regulation of PrPc. *Mol Cell Neurosci*. 2008;38(1):98–109.

39. Caughey B, Raymond GJ. The scrapie-associated form of PrP is made from a cell surface precursor that is both protease- and phospholipase-sensitive. *J Biol Chem*. 1991;266(27):18217–18223.

40. Borchelt DR, Taraboulos A, Prusiner SB. Evidence for synthesis of scrapie prion proteins in the endocytic pathway. *J Biol Chem*. 1992;267(9):6188–6199.

41. Daude N, et al. Knockout of the prion protein (PrP)-like Sprn gene does not produce embryonic lethality in combination with PrPC-deficiency. *Proc Natl Acad Sci U S A*. 2012;109(23):9035–9040.

42. Uchiyama K, Muramatsu N, Yano M, Usui T, Miyata H, Sakaguchi S. Prions disturb post-Golgi trafficking of membrane proteins. *Nat Commun*. 2013; 4:1846.

43. Moreno JA, et al. Sustained translational repression by eIF2alpha-P mediates prion neurodegeneration. *Nature*. 2012;485(7399):507–511.

44. Taraboulos A, Raeber AJ, Borchelt DR, Serban D, Prusiner SB. Synthesis and trafficking of prion proteins in cultured cells. *Mol Biol Cell*. 1992; 3(8):851–863.

45. Dron M, et al. Endogenous proteolytic cleavage of disease-associated prion protein to produce C2 fragments is strongly cell- and tissue-dependent. *J Biol Chem*. 2010;285(14):10252–10264.

46. Oliveira-Martins JB, Calella AM, Bridel C, Baumann F, Dametto P, Aguzzi A. Unexpected tolerance of α-cleavage of the prion protein to sequence variations. *PLoS One*. 2010;5(2):e9107.

47. Deleault NR, et al. Isolation of phosphatidylethanolamine as a solitary cofactor for prion formation in the absence of nucleic acids. *Proc Natl Acad Sci U S A*. 2012;109(22):8546–8551.

48. Deleault NR, et al. Cofactor molecules maintain infectious conformation and restrict strain properties in purified prions. *Proc Natl Acad Sci U S A*. 2012; 109(28):1938–1946.

49. Mallucci GR, et al. Targeting cellular prion protein reverses early cognitive deficits and neurophysiological dysfunction in prion-infected mice. *Neuron*. 2007;53(3):325–335.

50. Brandner S, et al. Normal host prion protein necessary for scrapie-induced neurotoxicity. *Nature*. 1996; 379(6563):339–343.

51. Aguzzi A, Falsig J. Prion propagation, toxicity and degradation. *Nat Neurosci*. 2012;15(7):936–939.

52. Choi EM, et al. Prion proteins in subpopulations of white blood cells from patients with sporadic Creutzfeldt-Jakob disease. *Lab Invest*. 2009; 89(6):624–635.

53. Zanusso G, et al. Prion protein expression in different species: analysis with a panel of new mAbs. *Proc Natl Acad Sci U S A*. 1998;95(15):8812–8816.

54. Kascsak RJ, et al. Mouse polyclonal and monoclonal antibody to scrapie-associated fibril proteins. *J Virol*. 1987;61(12):3688–3693.

55. Swietnicki W, Morillas M, Chen SG, Gambetti P, Surewicz WK. Aggregation and fibrillization of the recombinant human prion protein huPrP90-231. *Biochemistry*. 2000;39(2):424–431.

56. Kim C, et al. Protease-sensitive conformers in broad spectrum of distinct PrPSc structures in sporadic Creutzfeldt-Jakob Disease are indicator of progression rate. *PLoS Pathog*. 2011;7(9):e1002242.

57. Safar JG, et al. Transmission and detection of prions in feces. *J Infect Dis*. 2008;198(1):81–89.

58. Safar JG, et al. Measuring prions causing bovine spongiform encephalopathy or chronic wasting disease by immunoassays and transgenic mice. *Nat Biotech*. 2002;20:1147–1150.

59. Thackray AM, Hopkins L, Bujdoso R. Proteinase K-sensitive disease-associated ovine prion protein revealed by conformation-dependent immunoassay. *Biochem J*. 2007;401(2):475–483.

60. Bellon A, Seyfert-Brandt W, Lang W, Baron H, Gröner A, Vey M. Improved conformation-dependent immunoassay: suitability for human prion detection with enhanced sensitivity. *J Gen Virol*. 2003;84(pt 7):1921–1925.

61. Choi YP, Gröner A, Ironside JW, Head MW. Comparison of the level, distribution and form of disease-associated prion protein in variant and sporadic Creutzfeldt–Jakob diseased brain using conformation-dependent immunoassay and Western blot. *J Gen Virol*. 2011;92(pt 3):727–732.

62. McCutcheon S, Hunter N, Houston F. Use of a new immunoassay to measure PrPSc levels in scrapie-infected sheep brains reveals PrP genotype-specific differences. *J Immunol Methods*. 2005;298(1–2):119–128.

63. Mahal SP, Baker CA, Demczyk CA, Smith EW, Julius C, Weissmann C. Prion strain discrimination in cell culture: The cell panel assay. *Proc Natl Acad Sci U S A*. 2007;104(52):20908–20913.

64. Castilla J, Morales R, Saá P, Barria M, Gambetti P, Soto C. Cell-free propagation of prion strains. *EMBO J*. 2008;27(19):2557–2566.

65. Drisaldi B, et al. Genetic mapping of activity determinants within cellular prion proteins: N-terminal modules in PrPC offset pro-apoptotic activity of the doppel helix B/B' region. *J Biol Chem*. 2004; 279(53):55443–55454.

66. Vilette D, et al. Ex vivo propagation of infectious sheep scrapie agent in heterologous epithelial cells expressing ovine prion protein. *Proc Natl Acad Sci U S A*. 2001;98(7):4055–4059.

67. Moudjou M, et al. Glycan-controlled epitopes of prion protein include a major determinant of susceptibility to sheep scrapie. *J Virol*. 2004; 78(17):9270–9276.

68. Schneider CA, Rasband WS, Eliceiri KW. NIH Image to ImageJ: 25 years of image analysis. *Nat Methods*. 2012;9(7):671–675.